Breakdown and Combustion of JP-10 Fuel Catalyzed by Nanoparticulate CeO_2 and Fe_2O_3

Brian Van Devener and Scott L. Anderson*

Department of Chemistry, University of Utah, 315 South 1400 East Room 2020, Salt Lake City, Utah 84112

Received February 14, 2006. Revised Manuscript Received June 27, 2006

Thermal breakdown and oxidation of JP-10 (*exo*-tetrahydrodicyclopentadiene, $C_{10}H_{16}$), in the presence of nanoparticulate CeO_2 and Fe_2O_3, was studied in a small alumina flow-tube reactor on time scales around 1 ms. Decomposition products were analyzed by an in situ mass spectrometer. In the absence of any oxidizer, JP-10 pyrolyzes at temperatures above ∼900 K to a variety of hydrocarbon products. In the absence of O_2, both CeO_2 and Fe_2O_3 oxidize JP-10 efficiently, with decomposition onset temperatures up to 300 K lower than in a clean alumina flow tube under identical flow conditions and substantial conversion to products such as water, CO_2, CO, and formaldehyde. Under such noncatalytic conditions, the CeO_2 or Fe_2O_3 is reduced and deactivated by the reaction with JP-10. Decomposition of JP-10 in the presence of stoichiometric O_2 was also studied, with and without CeO_2 present. In absence of CeO_2, some oxidation products are observed; however, the rate-limiting step appears to be pyrolysis of JP-10, and pyrolysis products dominate for temperatures up to 1200 K. When both O_2 and CeO_2 are present, oxidation is clearly catalytic; i.e., oxidation is initiated by the reaction of JP-10 with CeO_2, which is then reoxidized by O_2.

1. Introduction

JP-10 (*exo*-tetrahydrodicyclopentadiene, $C_{10}H_{16}$) is a synthetic fuel, currently used in applications where high volumetric energy density is critical. Its heat of combustion (39.4 MJ/L) is substantially higher than petroleum-based fuels such as JP-8 (34.5 MJ/L). JP-10 is commonly used in combustion research,[1−14] at least partly because it is a single-component fuel and therefore much simpler to study than a petroleum distillate. One problem with JP-10, also affecting other liquid hydrocarbon fuels to varying extents, is that its ignition and combustion kinetics can be too slow for efficient combustion in applications such as pulse detonation engines or ramjets. Furthermore, while JP-10 has a volumetric energy density near the limit for readily synthesized liquid hydrocarbons, immediate benefits would accrue from the development of a fuel system with even higher energy density. We are interested in nanoparticle fuel additives for hydrocarbon fuels, designed to simultaneously enhance combustion rates and energy density. The idea is to have nanoparticles with a core of high energy density material, coated with a thin shell of a catalyst that accelerates ignition and combustion of the hydrocarbon (e.g., JP-10) carrier fuel. Palladium or other noble-metal-based catalysts are commonly used in catalytic combustors to increase the efficiency of combustion at low temperatures, thereby reducing NO_x production. For such applications, the reactant gases typically flow through a bed containing the catalyst immobilized on a high surface area support. For aircraft propulsion, this approach is ruled out by gas-flow velocity, contact time, size, and weight limitations. In the envisioned application, the catalyst-coated fuel particles will be injected into the combustor with the fuel and/or air and be consumed in the combustion process. For this reason, the catalyst must be inexpensive and have low toxicity as well. Here, we report the first studies of the catalytic combustion of JP-10, using nanoparticulate CeO_2 as the catalyst. A substantial reduction in the ignition temperature is observed, and it is demonstrated that initiation is by CeO_2 oxidation of JP-10, with O_2 serving primarily to close the catalytic cycle by reoxidizing the CeO_2. Fe_2O_3 nanoparticles are also shown to be active for JP-10 oxidation. Such catalysts could have wider applications than our core/shell nanoparticle approach, in coatings on engine surfaces, for example. The choice of JP-10 as the hydrocarbon fuel was largely to simplify mass spectrometric analysis. Qualitatively similar results are expected for other hydrocarbon fuels.

2. Experimental Design

The micro-flow-tube reactor mass spectrometer instrument used in these experiments has been described in detail elsewhere.[15−18] The design and operating conditions were modified for the catalysis

(1) Burdette, G. W. In *U.S.*; United States Department of the Navy, Washington, D.C., 1983; p 3.
(2) Antaki, P.; Williams, F. A. *Combust. Flame* **1987**, *67*, 1−8.
(3) Cho, S. Y.; Takahashi, F.; Dryer, F. L. *Combust. Sci. Technol.* **1989**, *67*, 37−57.
(4) Chung, H. S.; Chen, C. S. H.; Kremer, R. A.; Boulton, J. R.; Burdette, G. W. *Energy Fuels* **1999**, *13*, 641−649.
(5) Clausen, L. C.; Li, T. X.; Law, C. K. *J. Propul. Power* **1988**, *4*, 217−221.
(6) Guisinger, S. J.; Rippen, M. E. *Prepr.—Am. Chem. Soc., Div. Pet. Chem.* **1989**, *34*, 885−896.
(7) Peters, J. E.; Mellor, A. M. *J. Energy* **1982**, *7*, 95−96.
(8) Smith, N. K.; Good, W. D. *AIAA J.* **1979**, *17*, 905−907.
(9) Szekely, G. A., Jr.; Faeth, G. M. *Combust. Flame* **1983**, *49*, 255−259.
(10) Takahashi, F.; Dryer, F. L.; Williams, F. A. *Symp. (Int.) Combust., [Proc.]* **1988**, *21*, 1983−1991.
(11) Takahashi, F.; Heilweil, I. J.; Dryer, F. L. *Combust. Sci. Technol.* **1989**, *65*, 151−165.
(12) Wong, S. C.; Turns, S. R. *Chem. Phys. Processes Combust.* **1988**, 97/91−97/94.
(13) Wong, S. C.; Turns, S. R. *Combust. Sci. Technol.* **1989**, *66*, 75−92.
(14) Wong, S. C.; Lin, A. C. *Combust. Flame* **1992**, *89*, 64−76.
(15) Li, Z.; Anderson, S. L. *J. Phys. Chem. A* **1998**, *102*, 9202−9212.

10.1021/ef060064g CCC: $33.50
Published on Web 07/29/2006

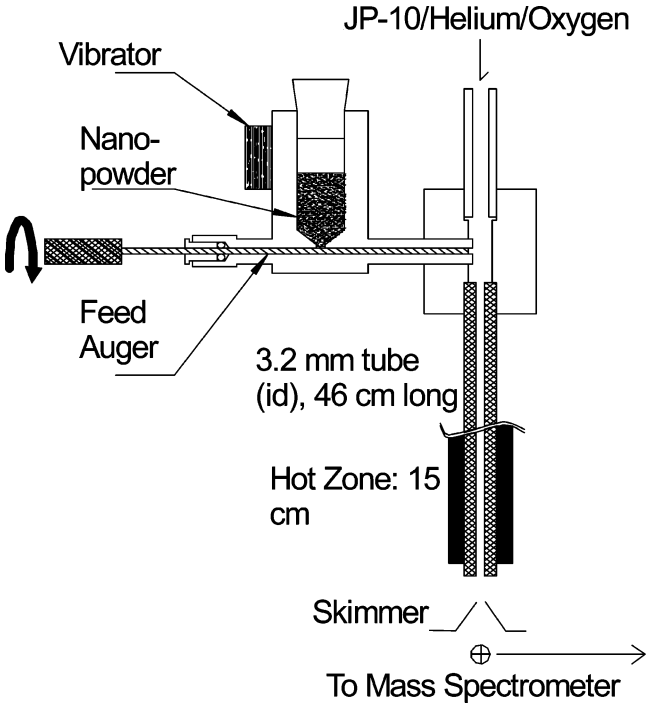

Figure 1. Nanoparticle feed mechanism.

experiments here, as described below. In essence, the instrument consists of a small flow-tube reactor, where chemistry is carried out, coupled to a tandem mass spectrometer for product detection and identification. The main changes were made to allow for higher flow rates and pressures and to enable the feeding of nanoparticles into the gas flow. Because the gas density is too low to carry the nanoparticles through the flow tube, the tube is oriented vertically, as shown in Figure 1. A 15 cm section, located 1 cm from the outlet end of the 46 cm long, 1.6 mm inner radius alumina flow tube, is heated by external tantalum windings and can reach temperatures as high as 1800 K. A standard K-type thermocouple is embedded into the wall of the tube to monitor temperature and is periodically calibrated against a thermocouple inserted into the flow-tube bore. The nanoparticle-laden gas stream exiting the flow tube is mostly pumped away by a large (40 L/s) mechanical pump, equipped with a particle trap to prevent nanoparticle contamination of the pump oil. The central portion of the gas stream is allowed to enter the differentially pumped ionization chamber through a 1 mm aperture in a skimmer cone, forming a molecular beam. The gas beam passes through an electron-impact ionization source and then into a 160 L/s diffusion pump located at the bottom of the ionization chamber. Ions are created by electron impact at an ionization energy of 75 eV, extracted along the horizontal axis, and analyzed by the tandem mass spectrometer instrument described previously.[15−18] Ionization chamber pressure is typically 5.5×10^{-5} Torr during operation.

For the measurements, either helium or O_2 is bubbled though a container of liquid JP-10 (Koch, ∼95%) at room temperature (vapor pressure of ∼2.6 Torr), with the gas pressure adjusted to give a gas mixture of either ∼3.9% JP-10 in helium or 6.67% JP-10 in O_2, with the latter being the stoichiometric ratio for combustion to CO_2 and H_2O. The gas mixture is then metered into the flow tube through a needle valve, to give a flow-tube entrance pressure of 20.1 Torr, as measured by a Baratron capacitance manometer. At the top of the flow tube, nanoparticles are introduced via a feed mechanism, consisting of an evacuated hopper containing the nanoparticulate powder and a motorized 2.89 mm diameter auger that delivers powder at a controlled rate from the hopper to a delivery ramp positioned above the flow-tube center line. To help feed particles smoothly, break up clumps, and disperse the powder across the flow-tube cross-section, the entire feed assembly is shaken by an electromechanical vibrator. The experiments used CeO_2 and Fe_2O_3 nanopowder from commercial sources. The CeO_2 (Nano-Scale Materials) had a specified average particle diameter of 120 nm, and the Fe_2O_3 (Sigma-Aldrich) had a specified average diameter of 20−25 nm. The average nanoparticle feed rate was typically ∼1.4 mg/s, determined by weight loss during the experiments. For reasons discussed below, the exact feed rate is not critical.

Table 1. Flow-Tube Properties

JP-10/He	300 K	900 K	1400 K
flow velocity (m/s)	16.4	34.8	45.4
mach number	0.02	0.02	0.02
hot zone midpoint pressure (Torr)	8.1	11.6	13.8
residence time (ms)	9.1	4.3	3.3
JP-10 diffusion speed (m/s)	2.2	6.1	8.9
average number of hot zone JP-10−wall collisions	12.4	16.4	18.3

$JP\text{-}10/O_2$	300 K	900 K	1400 K
flow velocity (m/s)	15.4	32.5	42.4
mach number	0.05	0.06	0.06
hot zone midpoint pressure (Torr)	8.1	11.6	13.8
residence time (ms)	9.8	4.6	3.5
JP-10 diffusion speed (m/s)	1.2	3.4	5.0
average number of hot zone JP-10−wall collisions	7.5	9.9	11.0

To understand the catalytic effects, it is important to review the properties of the flow-tube reactor. Table 1 summarizes the most important flow properties, calculated assuming incompressible flow. The inlet pressure at the top of the tube is typically set to 20.1 Torr. Because the hot zone is preceded by a room-temperature zone that is ∼200 tube radii long, very little adjustment of the gas-flow rate is needed to maintain constant inlet pressure, and fully laminar flow develops long before the hot zone. Assuming that the pressure at the outlet of the tube is equal to the vacuum chamber pressure (∼0.1 Torr), we estimate that the pressures at the beginning, midpoint, and end of the hot zone are 11.5, 8.1, and 2.1 Torr, respectively, for a flow-tube temperature of 298 K. The final 1 cm (≈6 tube radii) of the tube is unheated and clamped into a room-temperature holder, so that the large pressure drop near the tube outlet is spatially separated from the hot zone. The mass-averaged flow velocity is such that the average residence time for JP-10/He in the hot zone is ∼9.1 ms at 298 K, dropping to 3.3 ms at 1400 K. As indicated in the table, the residence time is slightly longer for the $JP\text{-}10/O_2$ mixture. The pressure at the hot zone midpoint is nearly identical for the two gas mixtures. Under these conditions, the mean free path for JP-10 collisions with the He or O_2 carrier is on the order of 10 μm, i.e., ∼200 times smaller than the tube radius. The corresponding JP-10 diffusion speed is such that the molecules diffuse across the flow tube on the order of 10 times during the hot zone residence time. This diffusion averages out the laminar flow velocity gradient, allowing the flow to be treated as pseudoplug flow, with uniform average residence times. Diffusion and wall collisions also ensure that the gas temperature closely follows the wall temperature, with rapid heating upon entering the hot zone. Finally, wall collisions provide a reproducible and easily characterized method to study chemistry in JP-10−nanoparticle collisions.

The latter point is important, because dry nanoparticulate powder is typically aggregated. In our case, the average CeO_2 nanoparticle size is 120 nm, but electron microscopy shows that the dry powder is aggregated into ∼5 μm grains. We have found that ultrasonication in liquid JP-10 breaks up the aggregates, providing means to achieve high dispersion in combustion applications. For the present dry-feed experiments, however, aggregation is unavoidable. Further-

(16) Li, Z.; Eckwert, J.; Lapicki, A.; Anderson, S. L. *Int. J. Mass Spectrom. Ion Processes* **1997**, *167/168*, 269−279.
(17) Nakra, S.; Green, R. J.; Anderson, S. L. In *15th ONR Propulsion Meeting*; Roy, G. D., Gupta, A. K., Eds.; Washington, D.C., 2002.
(18) Li, Z.; Anderson, S. L. *Adv. Chem. Propul.* **2002**, 61−76.

more, it is nontrivial to feed powder smoothly into a gas stream at the low pressures and flow rates possible in our instrument. As a consequence, it is difficult to achieve conditions where JP-10 makes a well-defined number of collisions with nanoparticles dispersed in the gas stream. Furthermore, at our low operating pressures, it is unclear if CeO_2 aggregates flowing in the gas stream would reach the wall temperature during the short hot zone residence time.

Fortunately, for our purposes, it is sufficient to have a controllable rate of JP-10−particle collisions at well-defined temperatures, and it is immaterial whether the particles are entrained in the gas flow or immobilized on the flow-tube walls. An obvious approach would be to simply coat the flow-tube walls with CeO_2 or Fe_2O_3 powder prior to use; however, interpretation would be complicated by possible changes in catalyst activity with time and operating conditions (see below). Our approach is to feed nanoparticles into the gas flow continuously, with the idea that enough will stick to the walls to provide a coating that is continually renewed with fresh material. Post-use examination of several flow tubes shows that nanoparticles do stick, generating a continuous coating that extends all along the tube length. For the feed rate and average aggregated particle size in these experiments, we can estimate that a few percent of particles sticking to the walls is sufficient to recoat the walls on a ~5 min time scale. Because catalyst deactivation occurs on a slower time scale even under strongly reducing conditions (see below), it is reasonable to assume that most of the wall surface is coated with active material. The catalyst coating builds up slowly during a series of experiments but is never allowed to grow to the point where it significantly changes the tube diameter, i.e., where it would affect the flow properties. Analysis of JP-10 encounter rates with free and immobilized particles is described below, but the result is that chemistry is dominated by the immobilized particles.

In our previous studies of pyrolysis of JP-10,[19,20] quadricyclane,[15] and cubanes,[21] we found that decomposition catalyzed by alumina and silica flow-tube surfaces was negligible, with the probable exception of dehydrogenation reactions occurring at temperatures well above those examined here. The lack of significant wall-catalyzed chemistry reflects the relative inertness of both silica and alumina. Moreover, we found that the silica and alumina surfaces quickly became coated by a thin gray carbonaceous layer. Once formed, this layer is stable for hundreds of hours of operation, and we speculated that it passivates the surface, reducing the wall reactivity. In the results below, we compare JP-10 decomposition for CeO_2- or Fe_2O_3-coated flow tubes to that observed under identical flow conditions for new (i.e., never exposed to catalyst) alumina flow tubes. Any differences in chemistry are clearly attributable to reactions on the CeO_2 or Fe_2O_3 particles.

Two types of mass spectral scans were used. To find the onset temperatures for JP-10 breakdown for different experimental conditions, the parent mass (136) was monitored continuously as the flow-tube temperature was stepped in ~10 K increments. Once the onset temperature was found, the product distribution was examined by taking full mass spectra at several temperatures above and below the breakdown onset. These mass spectra were taken with ~5 data points/atomic mass unit. To simplify a quantitative comparison of spectra, the intensities are plotted as "stick" spectra, where the height is proportional to the integrated intensity of each mass peak. The spectra were all normalized to constant total ion intensity for plotting. Fitting, described below, was then used to extract the composition of neutral species contributing to the mass spectrum at each temperature.

3. Results and Discussion

3.1. JP-10 Pyrolysis. Because our current flow tube differs in several respects from that used in our previous pyrolysis study, simple pyrolysis was recharacterized. Figure 2 shows a series of mass spectra of 3.9% JP-10 in He, taken after passage through a clean alumina flow tube at several different temperatures. No CeO_2 or Fe_2O_3 was present in these experiments. The bottom spectrum, for a 300 K flow-tube temperature, corresponds to intact JP-10 entering the ion source. There is a peak at the molecular mass (136); however, the spectrum is dominated by electron-impact-induced fragmentation, yielding a characteristic "fingerprint" pattern for JP-10. The extensive fragmentation is consistent with photoionization experiments by Federova et al.,[22] showing that a variety of C_5, C_6, C_7, C_8, and C_9 fragment ions have appearance energies within 1 eV of the JP-10 ionization threshold. The spectrum is also similar to what we previously reported,[19,20] and the differences in relative peak intensities are attributable to the rather different ion source used in those experiments.

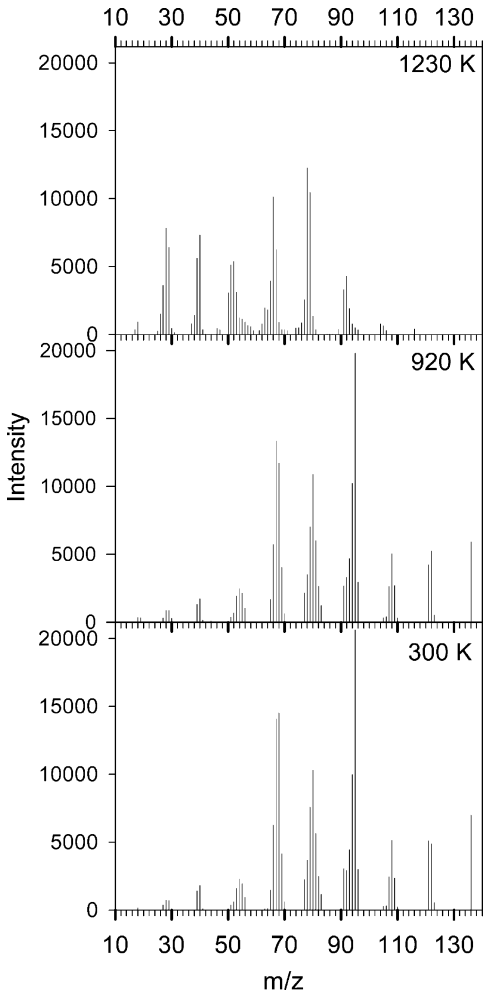

Figure 2. Pyrolytic breakdown of JP-10.

As the flow-tube temperature is increased, no mass spectral changes are observed for temperatures up to ~900 K, indicating that JP-10 remains intact on the millisecond time scale. The mass 136 intensity is observed to drop ~7% at 920 K, and examination of the corresponding mass spectrum also shows subtle changes in the relative intensities of some fragment peaks, indicating new contributions to these masses from ionization of JP-10 pyrolysis products. At higher temperatures, JP-10 is increasingly pyrolyzed, and by 1230 K, no JP-10 survives passage of the flow tube, as shown by the absence of the parent

(19) Nakra, S.; Green, R. J.; Anderson, S. L. *Combust. Flame*, in press.
(20) Green, R. J.; Nakra, S.; Anderson, S. L. In *Combustion Processes in Propulsion*; Roy, G. D., Ed.; Butterworth Heinemann: London, U.K., 2005; p 480.
(21) Li, Z.; Anderson, S. L. *J. Phys. Chem. A* **2003**, *107*, 1162−1174.
(22) Fedorova, M. S.; Denisov, Y. V.; Potapov, V. K. *Zh. Fiz. Khim.* **1973**, *47*, 2667−2670.

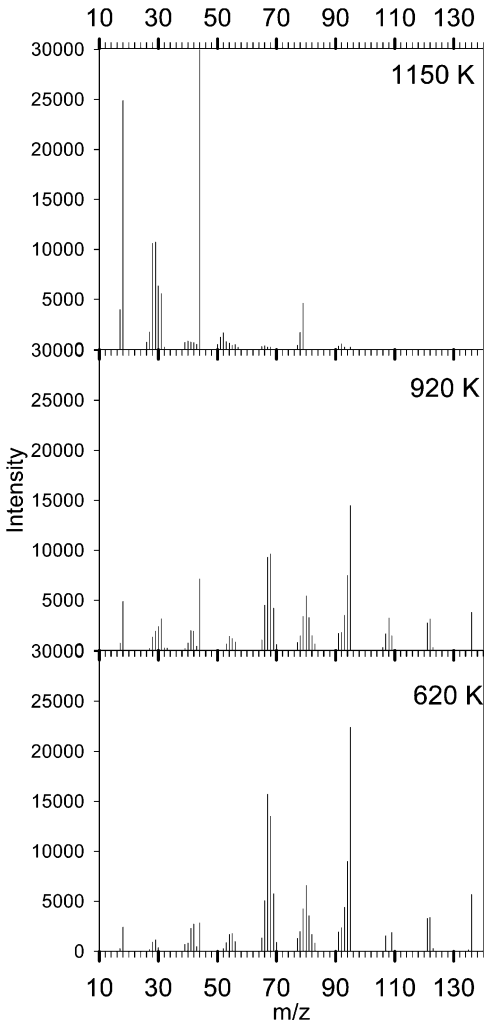

Figure 3. Breakdown of JP-10 with CeO_2.

peak (136). Evolution of the product distribution with temperature was explored in detail in our previous experiments,[19,20] and the similarity to the present results (see below) indicates that the pyrolysis chemistry is not significantly affected by our modest changes in flow-tube operating conditions.

These pyrolysis results provide a baseline against which the effects of CeO_2 or Fe_2O_3 nanoparticles can be evaluated. Figure 3 shows analogous plots for the breakdown of JP-10 in the presence of CeO_2 at 620 (just above the onset temperature), 920, and 1150 K flow-tube temperatures. The room-temperature spectrum is not shown, because it is essentially identical to that shown in Figure 2, where no CeO_2 was present. The implication is that room-temperature CeO_2 does not react with JP-10 nor catalyze its breakdown. A comparison of Figure 3 with Figure 2 shows that there is already more JP-10 breakdown at 620 K with CeO_2 than is observed at 920 K in absence of CeO_2. This breakdown is observed as intensity reductions for peaks characteristic of JP-10 (cf. masses above 100) and the appearance of product peaks, with the most obvious being 18 (water) and 44 (CO_2). At 920 K, the JP-10-characteristic peaks continue to decrease and peaks characteristic of products (18, 28−31, and 44) continue to grow. Finally, JP-10 is completely decomposed at 1150 K, i.e., about 100 K lower than in the absence of CeO_2. A comparison of the topmost spectra in Figures 2 and 3 shows that the product distribution is quite different, as well. In absence of any oxidizer (Figure 2), the products are all hydrocarbon fragments from pyrolysis. When CeO_2 is present, we might expect that the product distribution at 1150 K should contain both hydrocarbons from JP-10 pyrolysis and oxidation products from the reaction with CeO_2. As shown in Figure 3, however, oxidation is dominant and there is relatively little signal for hydrocarbon pyrolysis products (compare masses >50 in Figures 2 and 3).

To obtain a more quantitative understanding of the chemical species present during the breakdown of JP-10, it is necessary to fit the raw spectra, accounting for EI-induced fragmentation of the various neutral species present in the flow-tube exhaust stream. Fitting was done using a contracting grid, least-squares fit program and procedures described previously.[19] In essence, the spectra at each flow-tube temperature were fit to linear combinations of basis spectra for compounds known or suspected to be present. For the pyrolysis (i.e., CeO_2-free) spectra, the analysis assumed a product distribution similar to what was observed in our earlier study.[19,20] Basis spectra were included for C_2H_2 (acetylene), C_2H_4 (ethylene), C_3H_4 (propyne), C_5H_6 (cyclopentadiene), C_6H_6 (benzene), C_4H_x, C_7H_x, and the parent JP-10. For JP-10, the basis spectrum is simply the room-temperature EI spectrum (bottom of Figure 2), and for the various product species, the basis spectra were taken to be standard mass spectra present in the NIST Standard Reference Database.[23] The C_4H_x and C_7H_x basis spectra are synthetic spectra generated to fit the residual intensity in the 50−56 and 90−95 mass ranges, respectively, where no single molecule in the NIST database is capable of fitting the observed mass pattern.[19] For spectra obtained with CeO_2, Fe_2O_3, and/or O_2 present, we simply added basis spectra for water, CO, CO_2, and H_2CO to the set of hydrocarbon pyrolysis products. The raw fits give the contribution of each basis spectrum to the *ion* intensity distribution at each temperature. The results are given as the contribution of each *neutral* species to the product distribution at each temperature, correcting for the species dependence of EI detection efficiency, assuming linear scaling with the number of electrons in each molecule, as suggested by Flaim and Ownby[24] and Nishimura and Tawara.[25] We also include a series labeled "unfit residuals", which accounts for no more than 10% of the observed intensity at any temperature. The dominant contribution to the unfit residuals is discussed below.

Figure 4 (bottom frame) shows the product mole fraction distribution for pyrolysis of JP-10 as a function of the temperature, extracted from the fitting. For clarity, the JP-10 mole fraction is omitted from Figure 4 and plotted separately in Figure 5 to allow for a comparison of the breakdown under different experimental conditions. At 1150 K, i.e., the lowest temperature where there is enough decomposition to reasonably discuss the product distribution, the dominant products are benzene and cyclopentadiene (CPD), and benzene continues to be a major product at higher temperatures. CPD is, itself, unstable under our conditions at higher temperatures;[19] thus, its contribution to the product distribution diminishes, to be replaced by a variety of C_2, C_3, and C_4 products. There is additional secondary breakdown at higher temperatures; here, we restrict our attention to the temperature range below 1230 K, i.e., up to the point where no JP-10 survives.

Figure 4 (top frame) gives analogous fitting results for the breakdown in the presence of CeO_2, with the JP-10 breakdown

(23) Stein, S. E. In *NIST Chemistry WebBook*, NIST Standard Reference Database Number 69; Mallard, W. G., Linstrom, P. J., Eds.; NIST Mass Spec Data Center, National Institute of Standards and Technology: Gaithersburg MD, 2000 (http://webbook.nist.gov).

(24) Flaim, T. A.; Ownby, P. D. *J. Vac. Sci. Technol.* **1971**, *8*, 661−662.

(25) Nishimura, H.; Tawara, H. *J. Phys. B: At., Mol., Opt. Phys.* **1994**, *27*, 4401.

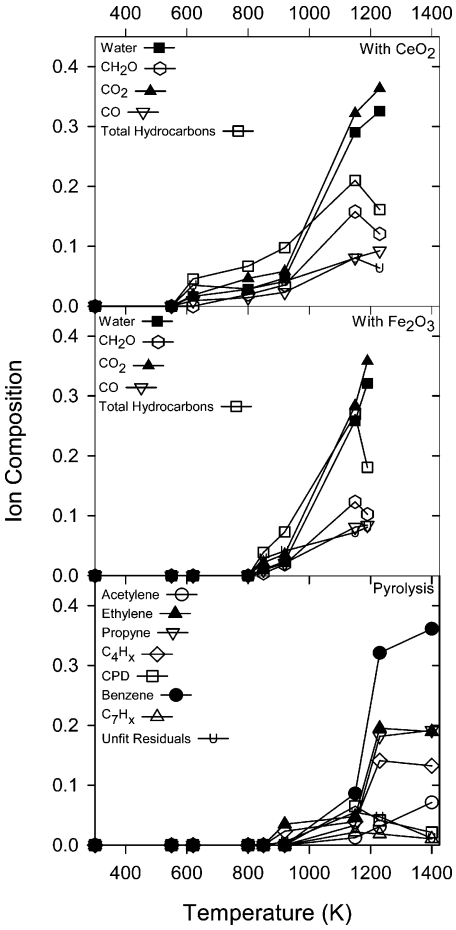

Figure 4. Breakdown products.

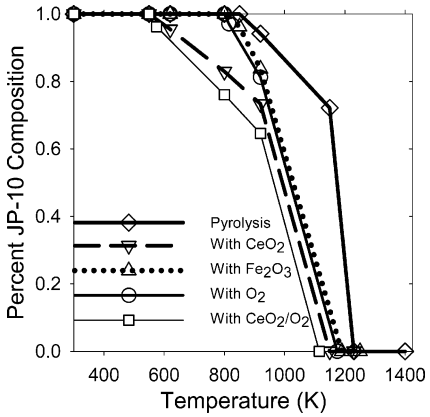

Figure 5. Percent JP-10 composition (various conditions).

behavior plotted separately in Figure 5. Figure 5 shows that decomposition sets in ~300 K lower temperature with CeO_2 than without and is also complete at ~100 K lower temperature. Figure 4 shows that water, CO, CO_2, and formaldehyde, i.e., oxidation products, account for ~85% of the product distribution at 1150 K. Within the considerable uncertainty that results from their small contribution to the spectra, it appears that the distribution of hydrocarbon products is consistent with simple pyrolysis. Note that there is ambiguity regarding the identification of some products. For example, mass 30 could have contributions from both ethane and formaldehyde. Because the pyrolysis mass spectra (Figure 2) have negligible mass 30 intensity, we attribute the bulk of the mass 30 appearing upon CeO_2 addition to formaldehyde. Similarly, propane shares the same mass as CO_2, but we assume that mass 44 in Figure 3 is

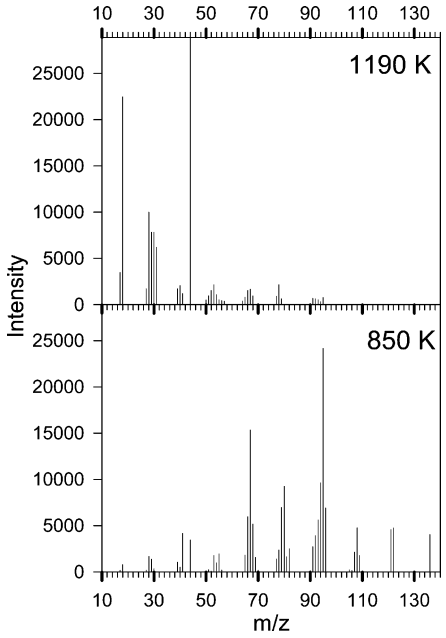

Figure 6. Breakdown of JP-10 with Fe_2O_3.

largely CO_2, because there is no evidence for propane in the pyrolysis product distribution (Figure 2). Mass 28 could be either C_2H_4 or CO, and a comparison of the intensity pattern for mass 26−28 suggests that both are present, in a ~2:1 ratio (CO/C_2H_4).

The only major mass peak without a clear assignment is mass 31 (CH_3O^+). Given that the rest of the peaks can be accounted for by EI of various stable molecules, the obvious assignment would be to an EI fragment ion from some heavier neutral product. The obvious candidates can, however, be ruled out from the mass spectra. For example, methanol fragments in EI to give a substantial intensity at mass 31, but it also gives substantial peaks at mass 32 (CH_3OH^+) and mass 15 (CH_3^+), neither of which is observed. Dimethyl peroxide and 1,2-ethanediol both give substantial mass 31 peaks under EI conditions; however, they can be ruled out by the observed absence of peaks at masses 62 and 33, respectively. Similar arguments apply to other candidate neutrals. Because mass 31 appears only when CeO_2 (or Fe_2O_3) is present, it is clear that the carrier of this signal must form by the reaction of JP-10 (or a JP-10 breakdown product) with the CeO_2 or Fe_2O_3 surface. In absence of any plausible alternatives, we tentatively attribute mass 31 to EI of a radical product, most likely CH_2OH ($\Delta H_f = -9$ kJ/mol)[26] or possibly CH_3O ($\Delta H_f = +17$ kJ/mol).[26] Because no standard mass spectrum exists for either radical,[23] the mass 31 signal is simply lumped into the unfit residuals, accounting for about half of the residual intensity for all experiments where CeO_2 or Fe_2O_3 was present.

3.2. JP-10 with Fe_2O_3. It is clear from the above results that CeO_2 can serve as an oxygen source at relatively low temperatures, oxidizing JP-10 well below the temperatures required for pyrolysis. CeO_2 is inexpensive and has relatively low toxicity. Nonetheless, it would be desirable to find an even cheaper and nontoxic material. For a comparison with CeO_2, Figure 6 presents analogous results for a (CeO_2-free) flow tube with Fe_2O_3 nanopowder being fed continuously, at a feed rate similar to that for the CeO_2 experiments. As with CeO_2, no

(26) Lias, S. G.; Bartmess, J. E.; Liebman, J. F.; Holmes, J. L.; Levin, R. D.; Mallard, W. G. In *NIST Chemistry WebBook*, NIST Standard Reference Database Number 69; Mallard, W. G., Linstrom, P. J., Eds.; National Institute of Standards and Technology: Gaithersburg, MD, 2000 (http://webbook.nist.gov).

decomposition is observed at low temperatures, in this case, up to ~800 K. The lower spectrum is for the lowest temperature where significant JP-10 decomposition was observed (850 K). The decomposition is most obviously shown by the presence of peaks for water and CO_2; however, a comparison with the bottom spectrum in Figure 2 shows some decrease in JP-10 intensity and other subtle changes as well. The top spectrum is for the first temperature (1190 K) where complete JP-10 decomposition was observed for Fe_2O_3. As in the CeO_2 case, the dominant products are water, CO_2, formaldehyde, and CO; however, there are also somewhat higher levels of hydrocarbon products than for CeO_2 in the same temperature range.

Figures 4 (middle frame) and 5 show the fitting results obtained for the Fe_2O_3-coated flow tube. Figure 5 indicates that the JP-10 breakdown behavior is intermediate between that of the alumina tube and the CeO_2-coated tube. The onset temperature for decomposition is only slightly lower than is observed for alumina tubes (i.e, for pyrolysis); however, the extent of decomposition increases more rapidly with temperature and is rather similar to the CeO_2 case for temperatures above ~950 K. At the onset of decomposition, hydrocarbon pyrolysis products dominate, but oxidation products such as water, CO, CO_2, and formaldehyde dominate at high temperatures. At 1190 K (the temperature where full JP-10 decomposition was observed), oxidized products such as water, CO_2, CO, and formaldehyde constitute about 75% of the product species, compared to ~85% for CeO_2 at 1150 K. The pattern suggests that Fe_2O_3 is relatively unreactive with intact JP-10 at temperatures up to the point where JP-10 pyrolysis begins; however, Fe_2O_3 clearly accelerates oxidative destruction of JP-10 at higher temperatures, presumably by reacting with both JP-10 and its pyrolysis products. As discussed next, the effects of Fe_2O_3 are strikingly similar to those seen when JP-10/O_2 mixtures are reacted in the absence of any active oxide coating of the reactor.

Although the effects of Fe_2O_3 and CeO_2 are similar for temperatures above 1150 K, Fe_2O_3 is considerably less active at initiating JP-10 breakdown at low temperatures, i.e., in the range expected to be most important for catalytic enhancement of hydrocarbon ignition and combustion. For this reason, catalytic JP-10 combustion and catalyst deactivation studies were only performed for CeO_2. Nonetheless, the activity observed for Fe_2O_3, combined with its low cost and toxicity, suggests that activity studies for other first-row transition-metal oxides are warranted.

3.3. JP-10 Combustion, with and without CeO_2. The above results show that CeO_2 will react with and oxidize JP-10, substantially reducing the onset temperature for decomposition. From a combustion perspective, the more important question is how effective CeO_2 is at catalyzing JP-10 ignition and combustion in JP-10/O_2 mixtures. To address this question, experiments similar to those above were carried out but with the helium carrier gas replaced by O_2. To simplify the analysis, we used JP-10 in pure O_2 with the JP-10/O_2 mixing fraction set to the stoichiometric ratio for complete combustion to CO_2 and water: $14O_2 + C_{10}H_{16} \rightarrow 10CO_2 + 8H_2O$.

JP-10 is an energetic fuel; thus, we might anticipate significant energy release under combustion conditions, possibly raising the flow-tube temperature for JP-10/O_2 relative to that for JP-10/He under similar heater power. There are several ways to estimate the possible temperature rise as a result of combustion. For the mass flow rate used here, complete combustion of the JP-10/O_2 mixture to CO_2 and H_2O would release ~7.9 W. Simply on the basis of the heat capacity of the gas mixture, this would result in a substantial temperature rise; however, as discussed above, diffusion leads to tens of wall collisions during the residence time and we expect that the gas temperature remains near that of the tube walls; i.e., the combustion energy is rapidly transferred to the walls, which have a very large heat capacity compared to that of the gas. Because we control the wall temperature, the measurements largely take this additional heating power into account. Because the combustion power is small compared to the heater power (~210 W in the middle of the experimental temperature range), the change in the heater power−temperature relation is small.

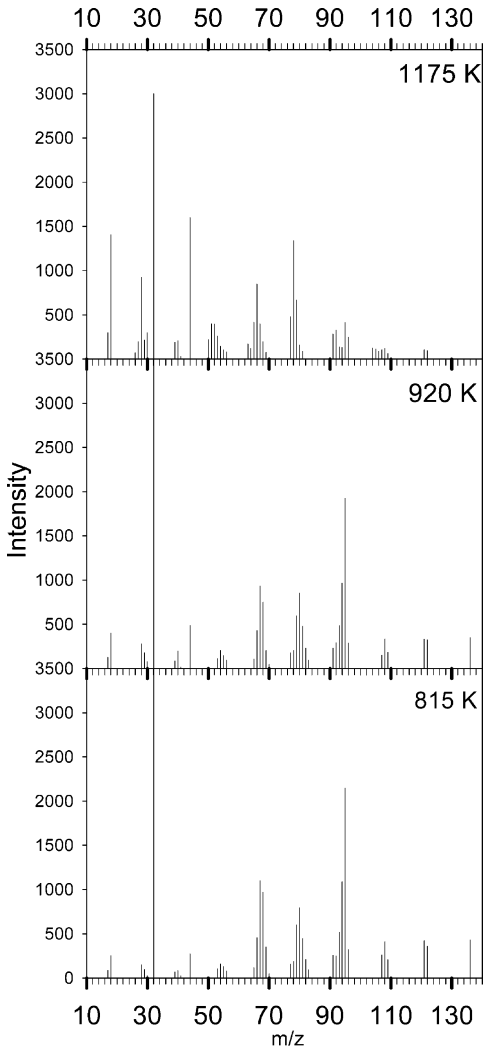

Figure 7. Breakdown of JP-10 with stoichiometric O_2 (no CeO_2).

Figure 7 shows the mass spectra resulting from passing the stoichiometric JP-10/O_2 mixture through the flow tube at 815, 920, and 1175 K, *with no CeO_2 catalyst present*. No reaction is observed at lower temperatures. These experiments were done with a new, CeO_2-free flow tube to ensure that any catalytic contribution comes only from the relatively inert alumina surface. It is useful to compare the JP-10 breakdown for JP-10/He and JP-10/O_2, in each case without CeO_2 (Figures 2 and 7). When O_2 is present, the temperature where significant JP-10 breakdown is observed decreases from ~920 to 815 K and the temperature required for complete JP-10 disappearance decreases from 1230 to ~1175 K. As shown in Figure 5, JP-10/O_2 is rather similar to JP-10/He with Fe_2O_3. Both have little effect on the initiation temperature for JP-10 decomposition but enhance breakdown (relative to pyrolysis) at higher temperatures. The two oxidizers differ, however, in that the fraction of fully oxidized products (H_2O, CO, and CO_2) at high

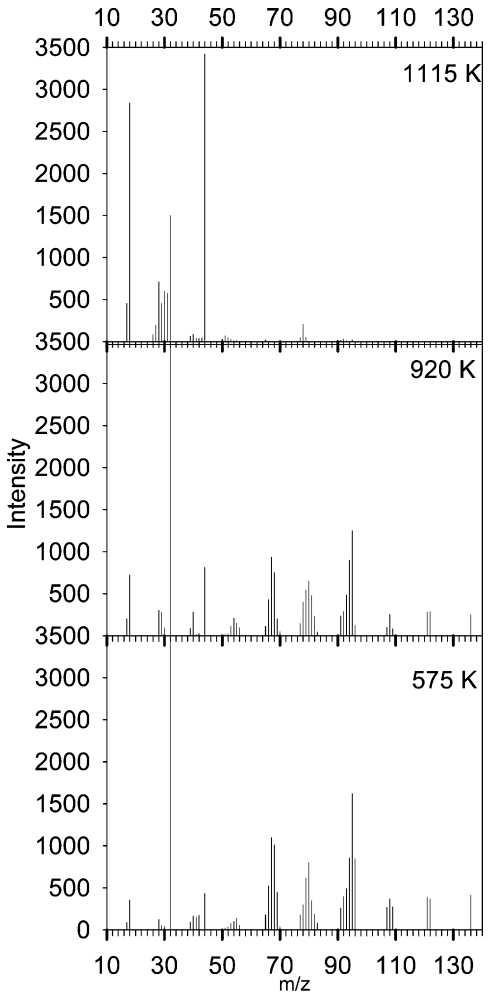

Figure 8. Breakdown of JP-10 with stoichiometric O_2 (with CeO_2).

temperatures is much smaller for O_2 than Fe_2O_3; i.e., the two oxidizers have similar efficiency for JP-10 decomposition, but Fe_2O_3 is more efficient at driving complete oxidation.

In pyrolysis (i.e., JP-10/He), JP-10 breakdown is obviously initiated by some isomerization or bond rupture event in JP-10. The slight decrease in the onset temperature for JP-10 breakdown in O_2, relative to JP-10/He, might tend to suggest that some reaction involving O_2 becomes rate-limiting when O_2 is present. In fact, we believe that JP-10 pyrolysis remains rate-limiting, even when oxygen is present. This conclusion rests on previous comparisons of decomposition behavior for JP-10/He with that for JP-10 in He with up to 10% O_2 added.[20] These O_2 levels are high enough to ensure that JP-10 collides frequently with O_2 in the hot zone but low enough that the gas-flow properties are not strongly modified. No changes in the onset temperature were observed in those experiments, although the temperature for complete JP-10 disappearance was reduced, as is observed in the present experiments. This observation suggests that JP-10 pyrolysis is the rate-limiting step but that additional reactions with O_2 accelerate JP-10 destruction once pyrolysis has begun.

The question is why the onset temperature observed here for JP-10 in stoichiometric O_2 is shifted to a lower temperature. One contributing factor is simply that the hot zone residence times for JP-10/O_2 are ~10% longer than those for JP-10/He, which would tend to allow for observable pyrolysis to occur at somewhat lower temperatures. A possible additional factor is that the presence of stoichiometric O_2 may increase the activity of the alumina flow-tube surface, by suppressing the formation

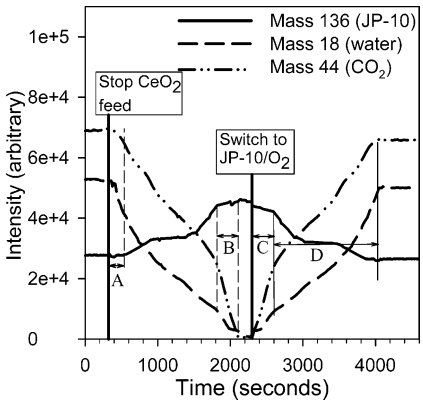

Figure 9. Catalyst reactivation.

of the carbonaceous layer observed for JP-10/He. The absence of an onset temperature shift in the experiments with O_2 diluted in helium is not surprising, because those mixtures were fuel-rich (equivalence ratio < 0.1), so that suppression of carbon deposition would not be expected. Regardless of the cause, the temperature shift is small compared to what is seen for JP-10/O_2 when CeO_2 is added.

Figure 8 shows mass spectra recorded for the case of JP-10/stoichiometric O_2, in the presence of CeO_2. In this case, JP-10 breakdown is significant already at 575 K, compared to 815 K with O_2 but without CeO_2, 620 K with CeO_2 but no O_2, and 920 K for simple JP-10 pyrolysis without either oxygen source. Furthermore, the JP-10 is completely gone at 1115 K, and at this temperature, the product distribution is almost entirely oxidation products, with only a few percent of residual hydrocarbons. A comparison of the CeO_2 results in Figure 5 for JP-10/O_2 and JP-10/He suggests that the onset temperature is not strongly affected by the presence of stoichiometric O_2. The small shift is probably attributable to a longer residence time for JP-10/O_2, as discussed above. This result indicates that the JP-10 reaction with CeO_2 is the rate-limiting step in both cases.

The above results show that both CeO_2 and O_2 can, by themselves, oxidize JP-10, with CeO_2 being the more active oxidizer. The key question is whether the enhanced oxidation chemistry observed when both O_2 and CeO_2 are present simply represents the additive effects of oxidation by CeO_2 and O_2 or if real catalytic oxidation is occurring. This point is important, because in any catalytic propulsion application, the goal would be to add the minimum amount of catalyst, because oxide catalysts would simply be dead weight, reducing the energy density of the fuel system. Two observations clearly show that real catalysis is occurring.

Compare the highest temperature spectra for JP-10/O_2 (Figure 7) and JP-10/O_2 with CeO_2 (Figure 8). If the much greater extent of oxidation in Figure 8 (compare residual hydrocarbon signal) were simply the effect of additional oxygen supplied by CeO_2, we should see a similar or smaller fraction of the initial O_2 consumed when CeO_2 is present. Instead, it can be seen that consumption of O_2 is more complete when CeO_2 is present; i.e., CeO_2 has catalyzed O_2 consumption and, by inference, JP-10 oxidation.

The catalytic effect can be seen more directly in experiments such as that summarized in Figure 9. Here, a JP-10/He flow was passed through the flow tube, with continual CeO_2 feed at 920 K, i.e, at a temperature where substantial JP-10 decomposition occurs only in the presence of active CeO_2. The intensities of the JP-10 parent (mass 136) and the major decomposition products (water and CO_2) were monitored to establish a baseline

for the amount of decomposition. The CeO_2 feed was then stopped while maintaining the JP-10/He gas flow, and changes in the parent and product intensities were continuously monitored. Note that the decomposition chemistry gradually stops; i.e., water and CO_2 disappear and the mass 136 signal increases. Eventually the signals reach a new steady state at ~2000 s, with no water or CO_2 production, and JP-10 intensity close to what would be observed for JP-10/He in a alumina tube at this temperature. Clearly, the reaction with JP-10 in the absence of O_2 completely deactivates the ceria coating on the tube walls on a ~2000 s time scale. The final step in the experiment was to switch the gas mixture to stoichiometric JP-10/O_2, leaving the CeO_2 feed turned off. Note that the mass 136 intensity decreases and the water and CO_2 intensities increase, with the system eventually reaching a new steady state after ~30 min. At steady state, the (CO_2 + H_2O)/JP-10 intensity ratio is almost identical to that seen when CeO_2 is being fed continuously. More importantly, the ratio is ~50% greater than that seen at this temperature for JP-10/O_2 in the absence of CeO_2 (Figure 7). The implication is that, at steady state, the CeO_2 coating remains catalytically active under stoichiometric conditions; i.e., it supplies oxygen to the JP-10, and the catalytic cycle is closed by O_2 reoxidizing the surface.

A close examination of Figure 9 provides additional insight into the deactivation and reactivation mechanisms. Note that the time dependence of the signals is more complex than might be expected if only a single deactivation/reactivation process were occurring. Instead, it is clear that both deactivation and reactivation occur in at least two steps, and even within the steps, the time dependence is not simple. For example, note that, when the CeO_2 flow is stopped, there is a ~250 s induction period before the JP-10 intensity begins to increase (time period A), whereas the CO_2 and H_2O signals both begin to decrease immediately. This behavior indicates that the CeO_2 layer continues to decompose JP-10 efficiently but is increasingly unable to supply enough oxygen to generated fully oxidized products. Given that the CeO_2 is reduced by the reaction with JP-10, such a loss of oxidizing capacity is not surprising. Note also that in the final period of deactivation (time period B), the JP-10 intensity has nearly reached the steady-state value, indicating that no decomposition is occurring, while CO_2 and H_2O continue to be produced, albeit with rapidly declining intensities. This pattern indicates that the tube walls are inactive for decomposition of JP-10 during this period but that they continue to evolve CO_2 and H_2O, presumably by the oxidation of hydrocarbons deposited on the walls earlier in the experimental sequence.

We conclude that CeO_2 deactivation results from two effects. The initial stage is gradual reduction of the ceria oxidation state, such that the surface becomes progressively less active. Initially, JP-10 still decomposes on the walls but not to fully oxidized products (time period A). As the ceria becomes less active, JP-10 decomposition and CO_2 and H_2O production continue to decrease (period around 1000 s). In the final stages of deactivation, we speculate that a carbonaceous film grows on the CeO_x surfaces, passivating them with respect to further JP-10 decomposition (period B). This film, in intimate contact with the CeO_x, continues to evolve CO_2 and H_2O to a diminishing extent, until the CeO_x is completely deactivated.

The reactivation phase of the experiment also supports the idea of a passivating carbonaceous layer. If the only source of CO_2 and H_2O were oxidation of JP-10, then the increase in CO_2 and H_2O intensities immediately after switching to the JP-10/O_2 mixture (time period C) should mirror the decrease in JP-10 intensity. Instead, the initial increase in CO_2 and H_2O signals is much more rapid than can be explained by JP-10 combustion. This pattern suggests that O_2 initially reacts primarily with the carbonaceous layer, generating CO_2 and, to a lesser extent, H_2O. Only after the carbonaceous layer is burned off, does O_2 begin to reactivate the underlying ceria, at which point the rate of JP-10 decomposition increases and the CO_2 and H_2O intensities come back in line with the JP-10 combustion stoichiometry (time period D). In considering stoichiometry, it is important to note that the intensities in Figure 9 are not corrected for relative ionization efficiency, which is roughly in the ratio 7.6:2.2:1 for JP-10, CO_2, and H_2O.

In evaluating the potential for catalytic combustion, a useful measure of activity is the JP-10 decomposition probability/encounter with a CeO_2 particle. To extract this number from the breakdown versus the temperature data (Figure 5), we need to estimate the number of encounters during passage through the hot zone, with both particles immobilized on the walls and particles flowing in the gas stream. Experiments where the particle feed is interrupted, such as that shown in Figure 9, provide a direct measure of the relative importance of free versus immobilized particles. While the CeO_2 is being fed, reactions can occur on both free and immobilized particles. Immediately after the particle feed is stopped, the reactivity of the immobilized particles is unchanged but flowing particles are no longer present. Therefore, the instantaneous change in the oxidation/total products ratio provides a direct measure of the relative importance of free and immobilized particles under our conditions.

Consider an interrupted feed experiment at 1150 K for JP-10 in helium, i.e., under conditions where the product distribution is exclusively hydrocarbons in the absence of CeO_2 and predominantly oxidized species (CO_2, H_2O, H_2CO, etc.) when active CeO_2 is present (top frame of Figure 3). In this experiment, there was an immediate ~13% drop in the signal for oxidized products when particle feeding was interrupted, implying that the reaction with CeO_2 immobilized on the walls generates ~8 times more products than the reaction with free-flowing CeO_2.

The measured CeO_2 feed rate can also be used to crudely estimate the relative importance of immobilized and free-flowing particles, and this estimate is a useful check on our interpretation of the interrupted feed experiments. Recall that both the free and immobilized particles are micrometer-scale aggregates of individual nanoparticles. The JP-10 mean free path between collisions is 10−50 μm under our conditions, larger than the average aggregate size (~5 μm) and much larger than the nanoscale structure of the aggregates. It is, therefore, not unreasonable to treat the aggregates as 5 μm spheres for the purpose of estimating JP-10−aggregate encounter rates. The nanostructure undoubtedly affects the reaction efficiency/JP-10−aggregate encounter; however, this effect should be similar for free and immobilized aggregates. If we assume that the tube walls are completely CeO_2-coated, as suggested by visual examination, the encounter rate is simply controlled by the area of the tube inner surface, ~100 mm^2/cm length of tube. On the basis of our measured particle feed rate (1.43 mg/s) and the electron microscopy estimate of the average aggregate diameter of ~5 μm, we can estimate that the surface area of free aggregates (neglecting the nanoscale structure) is about 17 mm^2/cm of flow-tube length. Crudely, therefore, the ratio of encounters with immobilized and free particles can be estimated to be ~6:1, in fair agreement with the 8:1 estimate from the interrupted feed experiments. Because the estimate derived from

Table 2. Probability of Decomposition/JP-10 Surface Encounter

JP-10/He on CeO_2

	620 K	800 K	920 K
JP-10−wall collisions	17.0	18.3	18.8
$\Delta F_{survive}$	0.954	0.823	0.792
P_{decomp} (%)	0.3	1.0	1.2

JP-10/He on Fe_2O_3

	620 K	800 K	920 K
JP-10−wall collisions	17.0	18.3	18.8
$\Delta F_{survive}$	1.00	1.00	0.896
P_{decomp} (%)	0.0	0.0	0.6

JP-10/O_2 on CeO_2

	620 K	800 K	920 K
JP-10−wall collisions	10.2	11.0	11.3
$\Delta F_{survive}$	0.912	0.761	0.833
P_{decomp} (%)	0.9	2.5	1.6

those experiments is more direct, we will use it in all further analyses.

Figure 5 shows that, for temperatures below 1000 K, there is substantially more JP-10 decomposition for flow tubes with CeO_2 or Fe_2O_3 coatings than for identical gas mixtures without the active oxide (cf. JP-10/He with and without CeO_2). When the amounts of decomposition occurring with and without active oxide present are subtracted, we can derive the corrected fraction ($\Delta F_{survive}$) of JP-10 that survives N_{col} collisions with active oxide in the flow-tube hot zone. The decomposition probability/encounter with a CeO_2 or Fe_2O_3 surface (P_{decomp}) is related to $\Delta F_{survive}$ as follows:

$$\Delta F_{survive}(T) = (1 - P_{decomp}(T))^{N_{col}(T)}$$

where N_{col} can be estimated from the JP-10 diffusion and flow properties (Table 1). This expression can be inverted to extract $P_{decomp}(T)$, and the results are given in Table 2. Note that the N_{col} numbers used in Table 2 are higher than those in Table 1, because they include a 15% correction for the effects of collisions with particles entrained in the gas stream.

Note that the P_{decomp} values are all in a relatively narrow range; however, this simply reflects the fact that P_{decomp} can only be extracted for temperatures where a significant fraction of the JP-10 survives.

From our sensitivity limit for detecting JP-10 survival (~0.1%), we can only say that P_{decomp} is greater than ~30% by 1150 K for both Fe_2O_3 and CeO_2, with or without O_2. The more interesting point is that significant P_{decomp} values occur at substantially lower temperatures for CeO_2, with or without O_2, than for Fe_2O_3. As expected, the values of P_{decomp} increase with increasing temperature, with one exception. For the case of JP-10/O_2 with CeO_2, P_{decomp} apparently decreases between 800 and 920 K; however, this effect is attributed to an artifact of the method used to correct for the background from pyrolysis. For JP-10/He, there is little decomposition in the temperature range up to 920 K; thus, the correction is small. As discussed above, the lack of decomposition in this temperature range is attributed to the formation of a passivating carbonaceous layer on the alumina walls. For JP-10/O_2, however, there is evidence that this passivating layer does not form (see above); thus, the P_{decomp} values for JP-10/O_2 with CeO_2 should be interpreted as the difference in decomposition between CeO_2 and unpassivated alumina. At 920 K, the results suggest that unpassivated alumina has significant activity for catalyzing JP-10 decomposition.

4. Summary

The mechanism for JP-10 decomposition, even in the absence of catalyst, is poorly understood. Williams et al.[27] have developed a reduced JP-10 mechanism that is reasonably successful at modeling JP-10 combustion behavior. On the other hand, attempts to model the product speciation in JP-10 pyrolysis using the reduced mechanism were unsuccessful[19] even when the mechanism is augmented with additional reactions taken from a mechanism developed for a JP-8 surrogate fuel by Violi et al.[28] In particular, the mechanism predicts a strong bias toward C_2 products and is unable to replicate the C_5 and C_6 products observed in pyrolysis. Because the combustion mechanism is so complex and is not completely understood even in absence of catalyst, we will focus this discussion on the effects of O_2, CeO_2, and/or Fe_2O_3 on the gross mechanism.

As discussed above, a comparison of results for JP-10/He and JP-10/O_2 without a catalyst suggest that initiation is controlled by JP-10 pyrolysis even when O_2 is present but that O_2 clearly accelerates decomposition once the temperature is high enough to initiate JP-10 breakdown. This result is not surprising. O_2 is a rather stable molecule; thus, both energy and entropic factors favor initial rupture of JP-10 bonds. In contrast, from a comparison of JP-10/He and JP-10/O_2 results with and without CeO_2, it is clear that, in the presence of CeO_2, the initiation step does change, significantly lowering the onset temperature. In contrast, Fe_2O_3 results in little reduction of the onset temperature for JP-10 breakdown, although it is an efficient oxidizer at higher temperatures.

In the absence of O_2, CeO_2 clearly functions as an oxidizer, but when O_2 is also present, the combustion reaction is clearly catalytic. The reaction with CeO_2 initiates the JP-10 breakdown process, and a subsequent reaction with O_2 restores the CeO_2 oxidation state. It is also clear that CeO_2 not only initiates JP-10 decomposition but also efficiently oxidizes the initial breakdown products, generating final products such as CO, CO_2, H_2O, and H_2CO. CeO_2 was chosen for this initial study based on the low cost and ready availability of nanoparticles; however, the results suggest that other reducible oxides may also be active JP-10 combustion catalysts.

Acknowledgment. This work was initially supported by the Office of Naval Research (N00014-01-1-0541).

EF060064G

(27) Williams, S.; Bench, P. M.; Midey, A. J.; Arnold, S. T.; Viggiano, A. A.; Morris, R. A.; Maurice, L. Q.; Carter, C. D. In *Proceedings of the JANNAF 37th Combustion, 25th Airbreathing Propulsion, 19th Propulsion Systems Hazards, 1st Modeling and Simulation Subcommittees Joint Meeting*; Naval Postgraduate School: Monterey, CA, 2000.

(28) Violi, A.; Yan, S.; Eddings, E. G.; Sarofim, A. F.; Granata, S.; Faravelli, T.; Ranzi, E. *Combust. Sci. Technol.* **2002**, *174*, 399−417.